J Physiol 592.5 (2014) pp 1119–1137

The Journal of Physiology

Sarcomere-length dependence of myosin filament structure in skeletal muscle fibres of the frog

Massimo Reconditi[1,2], Elisabetta Brunello[1], Luca Fusi[3], Marco Linari[1], Manuel Fernandez Martinez[4], Vincenzo Lombardi[1], Malcolm Irving[3] and Gabriella Piazzesi[1]

[1] *Laboratorio di Fisiologia, Dipartimento di Biologia, Università di Firenze, Via G. Sansone 1, 50019 Sesto Fiorentino, Italy*
[2] *Consorzio Nazionale Interuniversitario per le Scienze Fisiche della Materia, UdR Firenze, Firenze, Italy*
[3] *Randall Division, King's College London, London SE1 1UL, UK*
[4] *European Synchrotron Radiation Facility, BP220, F-38043 Grenoble, France*

Key points

- Contraction of skeletal muscle is thought to be regulated by a structural change in the actin-containing thin filaments of the sarcomere, but recent results have suggested that a structural change in the myosin-containing thick filaments may also be involved.
- We show that thick filament structure in resting muscle depends on the overlap with the thin filaments of the region of the thick filament containing myosin binding protein C (MyBP-C).
- During isometric contraction, the regions of the thick filaments that do not overlap with thin filaments are highly disordered, in contrast to their helical order in resting muscle.
- The results provide strong support for the role of a structural transition in the thick filaments, mediated by an interaction between MyBP-C and the thin filaments, in the physiological regulation of contraction in skeletal muscle.

Abstract X-ray diffraction patterns were recorded at beamline ID02 of the European Synchrotron Radiation Facility from small bundles of skeletal muscle fibres from *Rana esculenta* at sarcomere lengths between 2.1 and 3.5 μm at 4°C. The intensities of the X-ray reflections from resting fibres associated with the quasi-helical order of the myosin heads and myosin binding protein C (MyBP-C) decreased in the sarcomere length range 2.6–3.0 μm but were constant outside it, suggesting that an OFF conformation of the thick filament is maintained by an interaction between MyBP-C and the thin filaments. During active isometric contraction the intensity of the M3 reflection from the regular repeat of the myosin heads along the filaments decreased in proportion to the overlap between thick and thin filaments, with no change in its interference fine structure. Thus, myosin heads in the regions of the thick filaments that do not overlap with thin filaments are highly disordered during isometric contraction, in contrast to their quasi-helical order at rest. Heads in the overlap region that belong to two-headed myosin molecules that are fully detached from actin are also highly disordered, in contrast to the detached partners of actin-attached heads. These results provide strong support for the concept of a regulatory structural transition in the thick filament involving changes in both the organisation of the myosin heads on its surface and the axial periodicity of the myosin tails in its backbone, mediated by an interaction between MyBP-C and the thin filaments.

DOI: 10.1113/jphysiol.2013.267849

(Resubmitted 5 November 2013; accepted after revision 9 December 2013; first published online 16 December 2013)
Corresponding author M. Irving: Randall Division of Cell and Molecular Biophysics, King's College London, London SE1 1UL, UK. Email: malcolm.irving@kcl.ac.uk

Abbreviations AL1, first order actin-based layer line; C zone, region of the thick filament containing MyBP-C; ESRF, European Synchrotron Radiation Facility; FWHM, full width at half maximum; HA, high-angle peak of the M3 reflection; $I_{1,0}$, intensity of (1,0) equatorial reflection; I_{M1}, intensity of M1 reflection; I_{M3}, intensity of M3 reflection; I_{M5}, intensity of M5 reflection; I_{M6}, intensity of M6 reflection; LA, low-angle peak of the M3 reflection; MA, middle peak of the M3 reflection; M1, first-order myosin-based meridional reflection; M2, second-order myosin-based meridional reflection; M3, third-order myosin-based meridional reflection; M4, fourth-order myosin-based meridional reflection; M5, fifth-order myosin-based meridional reflection; M6, sixth-order myosin-based meridional reflection; ML1, first-order myosin-based layer line; MyBP-C, myosin binding protein C; R_{M3}, ratio of the intensities of the two peaks of the M3 reflection (higher angle/lower angle) during isometric contraction; S_{M2}, spacing of M2 reflection; S_{M3}, spacing of M3 reflection; S_{M5}, spacing of M5 reflection; S_{M6}, spacing of M6 reflection; T1, first-order troponin meridional reflection; $T_{0,2.1}$, plateau force reached during an isometric tetanus at sarcomere length 2.1 μm

Introduction

Contraction of vertebrate skeletal muscle cells is triggered by release of calcium ions from intracellular stores. The released calcium ions bind to the regulatory protein troponin in the actin-containing thin filaments of the muscle sarcomere, initiating azimuthal movement of a second regulatory protein – tropomyosin – around the thin filament. This in turn exposes the sites on actin to which the head domains of myosin molecules from the interdigitating thick filaments can bind and drive filament sliding (Ebashi *et al.* 1969; Gordon *et al.* 2000). Thus, the calcium-mediated regulatory switch for contractile activation in vertebrate skeletal muscle is considered to be intrinsic to the thin filaments, and essentially the same thin filament-based mechanism is present in cardiac muscle.

However, in smooth muscle and some invertebrate striated muscles the primary mechanism of contractile regulation involves structural changes in myosin molecules in the thick filaments mediated by phosphorylation of the myosin regulatory light chain. In these muscle types, myosin head domains are prevented from interacting with actin in the resting or dephosphorylated state by an interaction between the two heads of each myosin molecule to form a J-shaped motif close to the surface of the thick filament (Wendt *et al.* 2001; Woodhead *et al.* 2005). This J motif is seen not only in isolated myosin molecules from smooth muscle and in thick filaments from invertebrate skeletal muscle, but also in mammalian cardiac muscle (Zoghbi *et al.* 2008), and is probably also present in resting vertebrate skeletal muscle (Luther *et al.* 2011; Reconditi *et al.* 2011). These structural results suggest that an OFF state of the myosin molecule may have been conserved across the evolution of muscle types and species, and therefore that thick filament structure might also play a significant role in the regulation of contraction in vertebrate striated muscle.

The general idea of a regulatory role for the thick filaments in vertebrate skeletal muscle is not new, and was articulated in some detail by Haselgrove (1975) on the basis of the sarcomere length-dependence of the X-ray diffraction patterns from resting and active muscle, although the concept did not gain wide acceptance at the time. In recent years two main factors, in addition to the comparative structural approach described above, have led to renewed interest in the idea. Synchrotron sources now provide X-ray beams several orders of magnitude more intense than those available to Haselgrove in the 1970s, allowing diffraction patterns to be recorded with millisecond time-resolution during muscle force development. Such studies showed with increasing clarity that the structural changes in the thick filaments following activation are significantly faster than myosin binding to the thin filaments (Huxley *et al.* 1982; Lowy & Poulsen, 1990; Yagi, 2003; Brunello *et al.* 2006; Reconditi *et al.* 2011), suggesting the existence of a fast signalling pathway between the thin and thick filaments following the rise in intracellular free calcium concentration. Over the same period evidence accumulated from both skeletal and cardiac muscle for physical links between the thick and thin filaments mediated by myosin binding protein C (MyBP-C; Moos, 1981; Shaffer *et al.* 2009; Yamamoto, 1986; Luther *et al.* 2011). The physiological significance and function of such links remain controversial (Pfuhl & Gautel, 2012), but in principle they might provide a signalling pathway by which the state of the thin filament is communicated to the thick filament.

Here we set out to test the hypothesis that an interaction between MyBP-C and actin controls the structure of the thick filament and the conformation of the myosin heads in resting muscle. To do so, we took advantage of the fact that MyBP-C is confined to the 'C zones' of the thick filament, from 250 to 510 nm from the filament midpoint in fast skeletal muscles of amphibians (Bennett *et al.* 1986; Luther *et al.* 2008). Assuming a thin filament length of 1.0 μm, it follows that all the MyBP-C molecules

in the thick filament are in the thin filament overlap zone at sarcomere lengths less than about 2.5 μm (Fig. 1), that the overlap between the C zone and the thin filament is progressively lost between sarcomere lengths 2.5 and *ca* 3.0 μm, and that there is no possibility of MyBP-C-actin interactions at sarcomere lengths greater than *ca* 3.0 μm. We therefore recorded X-ray patterns from small bundles of intact muscle fibres at a series of sarcomere lengths at *ca* 0.1 μm intervals between 2.1 and 3.5 μm, and looked for structural changes in the thick filaments that were correlated with overlap between the C zone and the thin filaments. We made a similar series of measurements during steady isometric contraction over the same range of sarcomere lengths, to determine the effect of activation on the structure of the region of the thick filaments in which myosin heads cannot bind to actin and therefore cannot directly sense the structure of the thin filaments.

The characterisation of the conformations of the myosin heads that are not attached to actin in contracting muscle has broader significance for understanding the mechanism of muscle contraction itself, as well as that of its regulation. Most of the myosin heads, about 75%, are detached from actin during isometric contraction, and even more are detached during shortening (Piazzesi *et al.* 2007; Park-Holohan *et al.* 2012). The high fraction of detached heads is a fundamental determinant of muscle performance and efficiency, but the molecular factors controlling this parameter remain poorly understood. The present results allow a more detailed characterisation of the conformation of the detached heads in contracting muscle, and show that there are two populations with distinct conformations, each of which is also distinct from those of the actin-attached heads in contracting muscle and the detached heads in resting muscle.

The present experiments differ from the pioneering studies of Haselgrove (1975) and its antecedents (e.g. Elliott *et al.* 1963; Haselgrove & Huxley, 1973) in two important respects. We used a synchrotron X-ray source which, with optimized X-ray optics and detectors, provides an increase in the sensitivity of the measurements by several orders of magnitude. We also took advantage of the much higher X-ray flux to record the diffraction patterns from a population of sarcomeres of uniform length in a small bundle of 2–3 muscle fibres, avoiding the high passive stiffness and variable and inhomogeneous response to stretch of the whole muscles used in the previous studies.

Methods

Ethical approval

Frogs (*Rana esculenta*) were killed by decapitation and destruction of the brain and the spinal cord, following European Community Council Directive 86/609/EEC, and in conformity with the UK Animals Scientific Procedures Act, 1986.

Muscle fibres and experimental protocol

Bundles of two or, in a small minority of cases, three fibres *ca* 5 mm long were dissected from the tibialis anterior muscle and mounted via aluminium foil clips attached to the tendons in a trough containing Ringer solution (115 mM NaCl, 2.5 mM KCl, 1.8 mM $CaCl_2$, 3 mM phosphate buffer, pH 7.1) at sarcomere length 2.1 μm and 4°C. Sarcomere length in the different fibres from the same bundle differed by 2% or less, and in most cases by less than 1%. A pair of mica windows was positioned close to the fibre bundle, about 600 μm apart, to minimise the X-ray path in solution. Sarcomere length, fibre length and cross-sectional area were measured with a 40× water immersion objective and a 25× eyepiece. Force was measured with a capacitance transducer (Huxley & Lombardi, 1980). Isometric tetanic force was elicited using trains of stimuli of alternate polarity, frequency 20–25 Hz and duration 300–400 ms, delivered via platinum electrodes on the top and bottom edges of the opposing windows. Force, stimulus and X-ray acquisition timing were collected and analysed using LabVIEW (National Instruments, Austin, TX, USA).

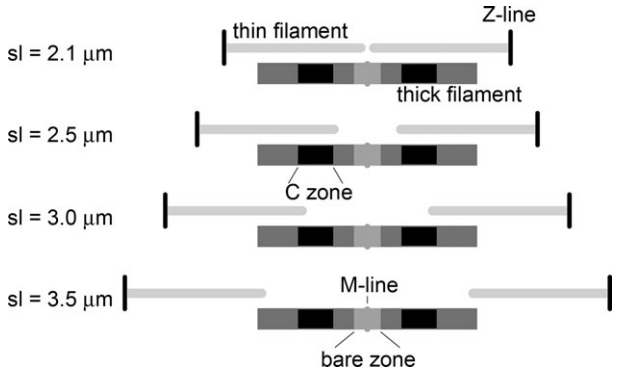

Figure 1. Overlap of thick filament regions with thin filaments at different sarcomere lengths
sl, sarcomere length.

X-ray data collection

The trough was sealed to prevent solution leakage, and the fibre bundle was mounted vertically at beamline ID02 of the European Synchrotron Radiation Facility (ESRF), which provided up to 6×10^{13} photons s^{-1} at 0.1 nm wavelength in a beam of size *ca* 300 μm (horizontal, full width at half maximum (FWHM)) and 150–250 μm (vertical) at the fibre bundle. The beam was attenuated for fibre bundle alignment. To minimise radiation damage, X-ray exposures of 1.6 or 10 ms duration were limited to

the data collection period using a fast electromagnetic shutter (nmLaser Products, Sunnyvale, CA, USA) and the fibre bundle was moved vertically by 0.1–0.2 mm between X-ray exposures. X-ray patterns during isometric contraction were recorded starting after 250 ms of stimulation in a tetanus. At the longer sarcomere lengths, associated with a biphasic time course of force development (Gordon *et al.* 1966), the X-ray exposure occurred after the rapid phase of force development, but before significant force 'creep'. Data were collected from up to 50 exposures in each bundle with no detectable sign of radiation damage. X-ray patterns were recorded with a high sensitivity fibre-optically coupled CCD detector (FReLoN) with an active area of 100 × 100 mm^2 (Sztucki *et al.* 2010), mounted 2.2 or 6 m from the fibre bundle. The 2048 × 2048 pixels of the CCD were unbinned in the vertical direction, but binned by eight in the horizontal direction before the readout to increase the signal-to-noise ratio.

Data analysis

X-ray diffraction data were analysed using the SAXS package (P. Boesecke, ESRF), Fit2D (A. Hammersley, ESRF) and Igor Pro (WaveMetrix, Inc., Lake Oswego, OR, USA). Two-dimensional patterns were centred and aligned using the equatorial (1,0) reflections, then mirrored horizontally and vertically. The distribution of diffracted intensity along the meridional axis of the X-ray pattern (parallel to the fibre axis) was calculated by integrating from 0.012 nm^{-1} on either side of the meridian for the myosin-based M3, M5 and M6 reflections, and 0.0046 nm^{-1} for the M1 and M2 reflections. The first myosin layer line (ML1) was integrated in the region between 0.064 and 0.037 nm^{-1} from the meridional axis. Background intensity distributions were fitted using a convex hull algorithm or straight-line fitting and subtracted; the small background remaining when the convex hull algorithm had been used was removed using the intensity from a nearby region of the X-ray pattern containing no reflections. Integrated intensities were obtained from the following axial regions: M3, 0.067–0.072 nm^{-1}; main peak of the M2 cluster, 0.0455–0.050 nm^{-1}; ML1, 0.015–0.023 nm^{-1} (low angle half of the ML1 reflection); M1, 0.021–0.024 nm^{-1}; M5, 0.113–0.120 nm^{-1}; M6, 0.137–0.142 nm^{-1}. The limits for ML1 were chosen to exclude the contribution of the first actin layer line. The profiles of the M2, M3, M5 and M6 reflections were fitted with Gaussian peaks from which the respective intensity and spacing were calculated; because of the complex but partially resolved shape of the M1 reflection, its intensity and spacing were calculated directly from the area and centroid of the observed meridional intensity distribution in the region 0.021–0.024 nm^{-1}. The cross-meridional widths of the meridional reflections were determined from Gaussian fits of the integrated radial intensity distribution in the axial regions defined above for each reflection; for the weaker reflections (M5, M6) this analysis could only be carried out on averaged X-ray patterns from multiple bundles. The reported values of the intensities of all meridional reflections have been corrected for the effects of lateral misalignment between filaments by multiplying the observed intensity by the cross-meridional width (Huxley *et al.* 1982), which increases with increasing sarcomere length due to a decrease in the degree of lateral alignment between adjacent thick filaments. For example, the width of the M3 reflection at rest (see supplementary Fig. S1*A*) was roughly constant in the sarcomere length range 2.1–2.6 μm, then increased by about a factor of three up to sarcomere length 3.2 μm, with no further increase at longer lengths. A similar sarcomere length dependence was observed during isometric contraction (Fig. S1*B*). The interference components of the M3 X-ray reflection were determined by fitting multiple Gaussian peaks with the same axial width to the meridional intensity distribution, and the total intensity of the reflection was calculated as the sum of the component peaks.

The spacing S of each reflection was determined from the weighted mean of that of the component peaks, $S_i = \lambda L/d_i$, where λ is X-ray wavelength, L the distance of the detector from the fibre bundle and d_i the distance of peak i from the centre of the pattern. The point-spread function of the FReLoN detector was *ca* 80 μm (FWHM), and the combined instrumental point spread function was negligible compared with the radial width of the meridional reflections. The intensity distribution on the equator of the X-ray pattern was determined by integrating from 0.0036 nm^{-1} on either side of the equatorial axis, and the intensity of the 1,0 reflection by fitting a Gaussian peak to the reflection.

The results reported below are from 18 fibre bundles (eight with a 6 m X-ray camera and 10 with 2.2 m), with mean (±SD) cross-sectional area 14,000 ± 4000 μm^2 and isometric plateau force at sarcomere length 2.1 μm ($T_{0,2.1}$) 175 ± 23 kPa. Measurements at rest and during isometric contraction in each bundle at each sarcomere length were paired, and made at the same location along the fibre, within 0.2 mm. This experimental design allowed all X-ray patterns to be normalised by the intensity of the (1,0) equatorial reflection in the resting state as described in Results.

Preliminary experiments showed that the axial and equatorial X-ray reflections from resting fibres at sarcomere length 2.1 μm became systematically weaker when measured after activation at a sarcomere length of 2.7 μm or greater. Fibres were therefore only stretched to sarcomere lengths of 2.7 μm or greater after completion of the measurements at shorter lengths. In general, there are fewer measurements at these longer sarcomere lengths, and the standard error of the mean is larger in this region.

Calculation of the intensity and interference fine structure of the M3 reflection from structural models

The intensity profile of the M3 X-ray reflection was calculated from structural models of the arrangement of myosin heads on the surface of the thick filament during isometric contraction, as described previously (Piazzesi *et al.* 2002, 2007; Reconditi *et al.* 2004; Brunello *et al.* 2007). Briefly, two myosin head arrays separated by a *ca* 160 nm bare zone were represented as 49 axial repeats of the average head conformation with *ca* 14.5 nm periodicity. In the no-overlap region of the sarcomere the average head conformation represents only detached heads, whereas in the overlap region it represents the fraction-weighted average of attached and detached heads; the axial periodicity is assumed to be the same in both regions. The attached head conformations during isometric contraction at 2.1 μm and 4°C in the two models described in Results (Brunello *et al.* 2007; Piazzesi *et al.* 2007) were modified to fit the interference fine structure of the M3 reflection measured in these conditions in *R. esculenta*, in which R_{M3} is *ca* 0.94, compared with *ca* 0.8 in *R. temporaria*. Taking into account the different fraction of actin-attached myosin heads (0.23 in *R. esculenta vs.* 0.30 in *R. temporaria*; Park-Holohan *et al.* 2012) and the different force and myofilament strain in the two species, we adjusted the tilt angle θ of the lever arm of the actin-attached heads to fit the R_{M3} value measured in *R. esculenta*, assuming that the bare zone is the same size in the two species. The alternative assumption, that θ is the same in the two species and the different values of R_{M3} are due to a different bare zone length, gave essentially the same results.

Results

Low-angle muscle X-ray patterns at different sarcomere lengths

The left-hand quadrants in Fig. 2*A* and *B* show examples of X-ray patterns recorded from small bundles of muscle fibres at rest at sarcomere length 2.1 μm (upper), with maximum overlap between thick and thin filaments, and 2.7 μm (lower), where overlap has been reduced by about 40%. The equatorial (1,0) and (1,1) reflections from the hexagonal array of filaments are further from the centre of the pattern at the longer sarcomere length, indicating compression of the hexagonal lattice of thick and thin filaments in the overlap zone of the sarcomere (Matsubara & Elliott, 1972; Haselgrove & Huxley, 1973). Although this effect was not a focus of the present study, the results allowed a precise characterisation of the relationship between lattice spacing and sarcomere length both at rest and during isometric contraction (see Supplementary Information and Figs S2 and S3). Lattice compression with increasing sarcomere length is accompanied by little change in the intensity of the (1,0) reflection associated with the planes of the hexagonal lattice passing through the centres of adjacent thick filament layers.

Most of the meridional reflections along the vertical axis of Fig. 2*A* and *B* index on an axial periodicity of *ca* 43 nm. Following convention, we refer to these as 'myosin-based' reflections, so the meridional reflection corresponding to the 43 nm periodicity will be called the M1 reflection and its higher orders M2, M3, etc. However, other thick filament components are likely to contribute to these reflections, and MyBP-C in particular makes a significant contribution to the M1 reflection (Rome *et al.* 1973; Huxley *et al.* 2009; Luther *et al.* 2011). The myosin-based meridional reflections M1–M6 are weaker at sarcomere length 2.7 μm than at 2.1 μm in resting fibres (Fig. 2*C*). This is mainly due to the fact that, when the muscle fibres are stretched, a smaller number of sarcomeres are illuminated by the fixed-size X-ray beam, and a normalisation procedure for this effect is described in the next section.

At the plateau of an isometric tetanus (Fig. 2*A* and *B*, right quadrants; Fig. 2*D*), the M1 reflection associated with MyBP-C, the M3 associated with the axial periodicity of the myosin heads and the M6 associated with the thick filament backbone remain strong, but the first myosin layer line (ML1) and the M2, M4 and M5 meridional reflections associated with the quasi-helical packing of the myosin heads on the surface of the thick filaments become very weak (Huxley & Brown, 1967; Huxley *et al.* 1982; Piazzesi *et al.* 1999; Brunello *et al.* 2006; Reconditi *et al.* 2011). The intensities of the M1 and M6 reflections are similar at sarcomere lengths 2.1 and 2.7 μm (Fig. 2*D*), whereas the M3 reflection is weaker at the longer sarcomere length.

Normalisation of X-ray patterns recorded at different sarcomere lengths

A precise normalisation for the diffracting mass in the X-ray beam was achieved by dividing each pattern by the intensity of the (1,0) equatorial reflection in the resting fibre bundle at each sarcomere length. This normalisation also removes the effect of cross-sectional area on diffracted intensities, so that results from different bundles, or different regions along a single bundle, can be directly combined or compared. The validity of this normalisation procedure depends on the hypothesis that the intensity of the (1,0) reflection ($I_{1,0}$) in resting muscle does not depend on sarcomere length *per se*, but only on the number of filaments in the X-ray beam at any sarcomere length.

This hypothesis is supported by the results and analysis presented in Fig. 3. First, resting $I_{1,0}$ at sarcomere length 2.1 μm recorded from different fibre bundles was directly

proportional to the isometric force generated when that bundle was maximally activated by repetitive electrical stimulation at that sarcomere length ($T_{0,2.1}$; Fig. 3*A*). The regression line through these data has an intercept on the intensity axis not significantly different from zero ($P \approx 0.05$, d.f. $= 16$). Thus, to a good approximation fibre bundles with a larger cross-sectional area, with more filaments in parallel and thereby producing greater active force ($T_{0,2.1}$), have a proportionally larger value of resting $I_{1,0}$. $T_{0,2.1}$ is preferred to cross-sectional area as an estimate of the number of filaments contributing to the diffraction pattern because it can be measured with greater accuracy. Resting $I_{1,0}$ divided by $T_{0,2.1}$ therefore gives a reliable normalisation for $I_{1,0}$ that does not depend on the size of the bundle. This parameter decreased linearly with increasing sarcomere length (Fig. 3*B*), as the number of sarcomeres and therefore the number of filaments in the fixed-size X-ray beam decreases. If there were no intrinsic effect of sarcomere length on resting $I_{1,0}$, the measured $I_{1,0}$ divided by $T_{0,2.1}$ and multiplied by sarcomere length would be independent of sarcomere length, and this was found to be the case (Fig. 3*C*). Linear regression of the data in Fig. 3*C* gave a slope of 0.014 ± 0.065, which is not significantly different from zero. We conclude that resting $I_{1,0}$ does not depend on sarcomere length *per se*, and can therefore be used to normalise the X-ray patterns for the

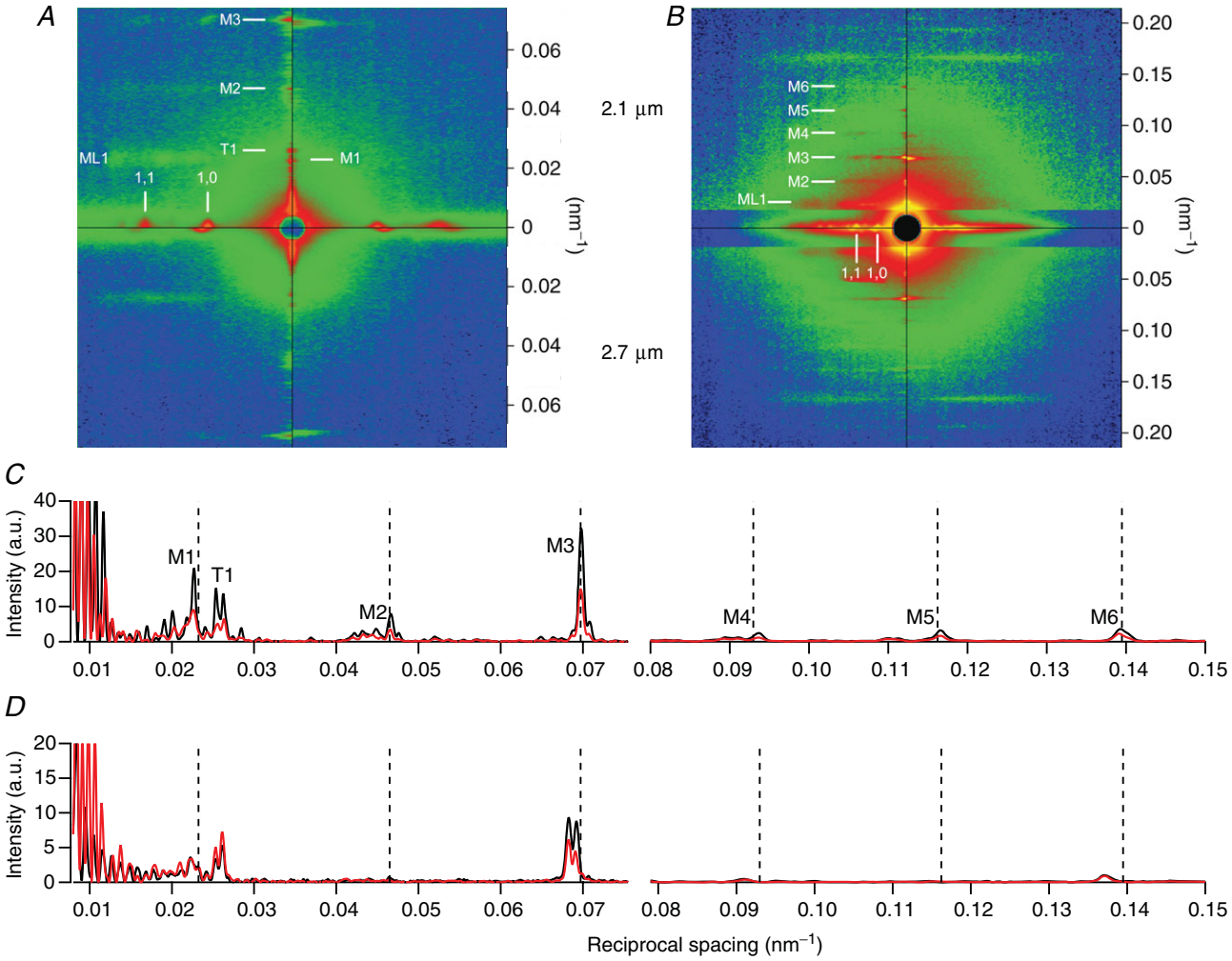

Figure 2. Low-angle X-ray diffraction patterns from a bundle of two intact muscle fibres
The left quadrants of *A* (6 m camera) and *B* (2.2 m camera) were recorded from resting fibres and the right quadrants during isometric contraction. Upper quadrants, sarcomere length 2.1 μm; lower quadrants, 2.7 μm. The fibre axis is vertical. Exposure times: 5 ms (*A*); 20 ms (*B*, 2.1 μm); 40 ms (*B*, 2.7 μm, but counts divided by 2 for comparison with 2.1 μm). In *B* the equatorial region has been digitally attenuated. The ordinate scale denotes reciprocal spacing. Intensity distributions along the meridian are shown in *C* (rest) and *D* (isometric contraction); data from reciprocal spacings less than 0.075 nm^{-1} are from *A* and the remainder from *B*; black line 2.1 μm, red line 2.7 μm. Vertical dashed lines indicate the 43.02 nm periodicity and its higher orders.

number of filaments in the X-ray beam at any sarcomere length. All the X-ray intensity data presented below have been so normalised.

Sarcomeric X-ray reflections

The very low parasitic or background scatter of the ID02 X-ray camera at ESRF allowed the intensities of meridional reflections very close to the beam-stop, corresponding to periodicities of *ca* 160–80 nm, to be recorded with high signal-to-noise both at rest (Fig. 2*C*, Fig. S4*A*) and during isometric contraction (Fig. 2*D*; Fig. S5). These reflections correspond to orders of the half-sarcomere length (Bordas *et al.* 1987) and therefore allow the sarcomere length in the region of the fibre illuminated by the X-ray beam to be determined directly from the X-ray data. This procedure gave reproducible results for sarcomere lengths up to 2.9 μm and in some cases 3.2 μm, with the measured periodicity in good agreement with the half-sarcomere length (Figs S4*B* and S5), but failed at longer lengths, at which the sarcomere-related periodicity was replaced by a length-independent periodicity of *ca* 950 nm, the structural basis of which is unknown. The sarcomere length during isometric contraction was the same as that at rest, within the resolution of the measurements. The abrupt loss of the sarcomere reflections at sarcomere lengths of 2.9–3.2 μm may be due to sarcomere length inhomogeneity associated with the resting tension in the strained cytoskeleton (Fig. S4*C*).

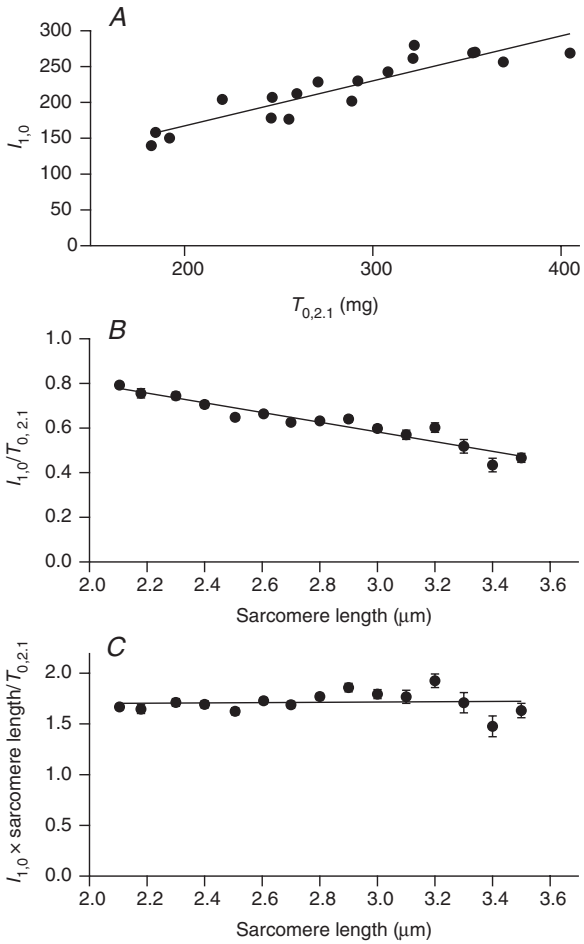

Figure 3. Use of the intensity of the equatorial (1,0) reflection ($I_{1,0}$) from resting fibres for normalization of the X-ray patterns
A, resting $I_{1,0}$ at sarcomere length 2.1 μm (arbitrary units) plotted against the isometric force generated at that sarcomere length ($T_{0,2.1}$); each point is from a different fibre bundle. *B*, resting $I_{1,0}$ normalized by $T_{0,2.1}$ in each bundle and plotted against sarcomere length (mean ± SEM from a total of 18 bundles, n = 2–9 bundles for each point). *C*, the normalized data in *B* multiplied by sarcomere length and plotted against sarcomere length; the regression line through these data has a slope of 0.014 ± 0.065.

The M3 reflection associated with the axial repeat of the myosin heads

In resting fibres, the intensity of the M3 reflection, I_{M3}, was approximately independent of sarcomere length over the whole range studied (Fig. 4*A*, circles), after correction for changes in its cross-meridional width (see Methods). Thus, the axial mass distribution of the myosin heads along the thick filaments signalled by the M3 reflection is independent of filament overlap in resting muscle. Moreover, the interference fine structure of the M3 reflection (insets in Fig. 4*A*), observed as the higher angle (HA) peak or shoulder on the right-hand side of the main M3 peak (MA), and the low angle (LA) peak or shoulder on the left, is also independent of sarcomere length. The relative intensities of the HA, LA and MA peaks have no detectable dependence on sarcomere length up to 2.9 μm, the largest sarcomere length at which multiple peak-fitting of the reflection profile was reliable (Fig. S6). The spacing of the M3 reflection at rest, S_{M3}, is roughly constant in the sarcomere length range 2.1–2.6 μm, increases in the range 2.6–3.0 μm, and then is constant again from 3.0 to 3.4 μm (Fig. 4*D*, open circles).

During active isometric contraction, the intensity of the M3 reflection, I_{M3} (Fig. 4*B*, filled circles) decreases linearly with increasing sarcomere length in the range 2.1 to *ca* 2.9 μm, and linear regression of these data (continuous line) indicated a best-fit relationship intersecting the sarcomere length axis at 3.56 ± 0.07 μm. This relationship matches the sarcomere length-dependence of active isometric force (triangles), which had a similar regression intercept, 3.62 ± 0.03 μm, consistent with the well-known linear dependence of active isometric force on the degree of overlap between the thick and thin filaments (Gordon *et al.* 1966). Thus, in the sarcomere length range 2.1 to *ca* 2.9 μm, the intensity of the M3 reflection is also

directly proportional to the degree of overlap between the thick and thin filaments, suggesting that it is primarily due to actin-attached myosin heads in the overlap zone (Linari *et al.* 2000). The simple relationship between I_{M3} and sarcomere length breaks down at sarcomere lengths greater than 2.9 μm and is difficult to measure reliably in highly stretched fibres. The cross-meridional width of the M3 reflection was almost constant in the sarcomere length range 2.1–2.7 μm, then increased at longer sarcomere lengths (Fig. S1*B*), indicating that lateral alignment between adjacent thick filaments is reduced during isometric contraction at those longer lengths.

During isometric contraction at sarcomere length 2.1 μm, the axial profile of the M3 reflection (Fig. 4*B*, insets) has two main peaks, with the higher angle (rightmost) peak having a slightly lower intensity (Linari *et al.* 2000). These peaks are due to sampling of the M3 reflection by a fringe pattern produced by X-ray interference between the arrays of myosin heads in the two halves of each thick filament. At longer sarcomere lengths, the intensity of both peaks decreases together, until the measurements become unreliable at sarcomere length 3.1 μm and above. The ratio R_{M3} of the intensities of the two peaks of the M3 reflection (higher angle/lower angle) is very sensitive to movements of the myosin heads along the thick filament (Piazzesi *et al.* 2002). R_{M3} was independent of sarcomere length in the range 2.1–2.9 μm (Fig. 4*C*). Linear regression of the R_{M3} data in this range gave a slope of -0.115 ± 0.086 (mean $\pm$ SEM, $n = 8$), which is not significantly different from zero.

At sarcomere length 2.1 μm, the spacing of the M3 reflection, S_{M3}, is about 1.6% larger during isometric contraction than at rest (Huxley & Brown, 1967; Linari *et al.* 2000). S_{M3} during isometric contraction was independent of sarcomere length in the range 2.1–2.8 μm, then started to decrease at longer sarcomere lengths (Fig. 4*D*, filled circles), in contrast with the *increase* in S_{M3} with increasing sarcomere length in resting muscle (open circles).

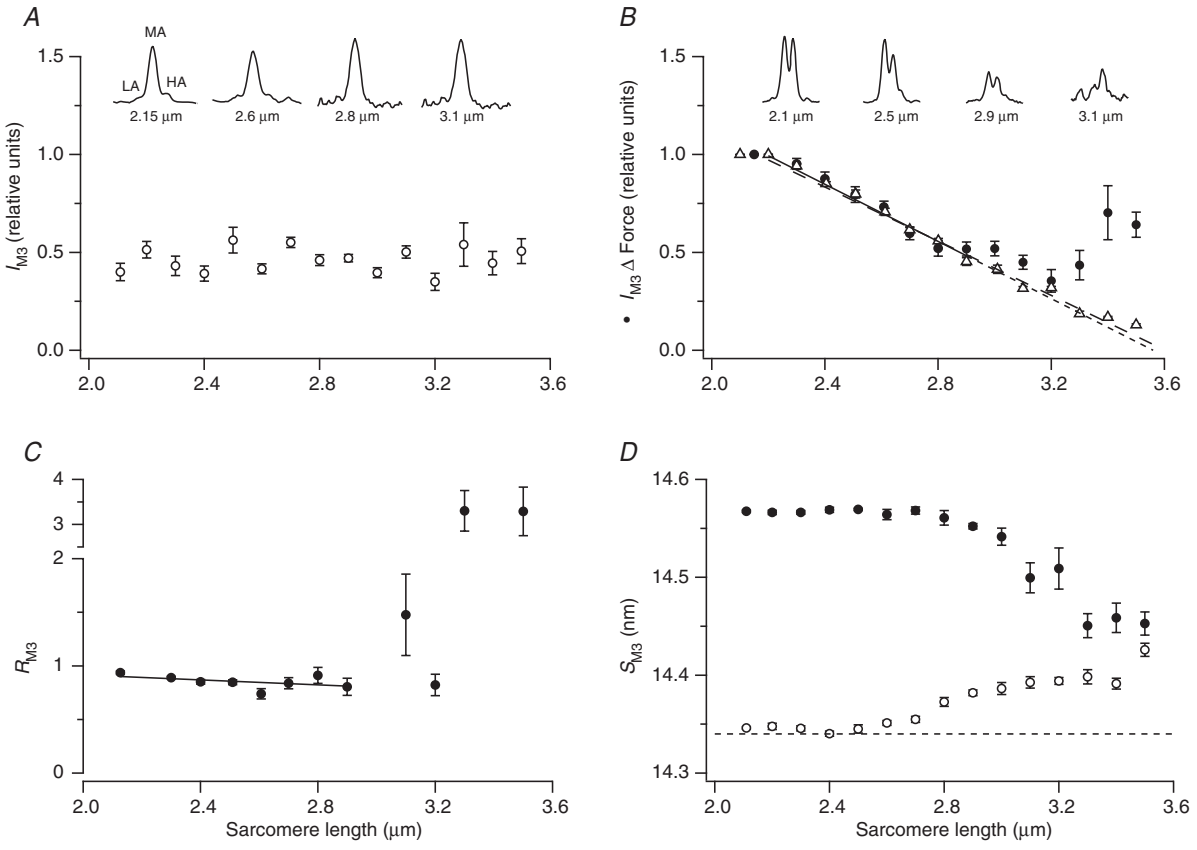

Figure 4. Sarcomere-length dependence of the M3 reflection
A, intensity of the M3 reflection, I_{M3}, at rest. *B*, I_{M3} (filled circles) and isometric force (triangles) during isometric contraction; the regression line for I_{M3} in the range 2.1–2.9 μm is the continuous line (extrapolated as the short-dashed line); that for force is the long-dashed line. The insets in *A* and *B* show the axial profiles of the M3 reflection at the indicated sarcomere lengths. *C*, ratio (R_{M3}) of the higher and lower angle peaks of the M3 reflection during isometric contraction; the regression line in the range 2.1–2.9 μm (continuous line) has slope -0.115 ± 0.086 μm^{-1}. *D*, spacing of the M3 reflection (S_{M3}) at rest (open circles) and during isometric contraction (filled circles) recorded in the same fibre bundles.

Conformation of the myosin heads during isometric contraction

To derive a quantitative description of myosin head conformations during isometric contraction in different regions of the thick filament from the above results, we adapted an approach used previously to interpret changes in the X-ray reflections produced by applying rapid decreases of muscle length during active contraction (Irving *et al.* 2000; Piazzesi *et al.* 2002; Reconditi *et al.* 2004; Huxley *et al.* 2006). This shortening-step protocol synchronises the motions of the actin-attached heads with relatively little change in the number attached, and provides a description of their conformation. The present results allow this approach to be extended to the larger population of detached heads.

The shape of the myosin heads is taken from X-ray crystallography (Rayment *et al.* 1993*a*; Fig. 5*A*). The catalytic domain of the actin-attached heads is assumed to be able to bind to actin in the same conformation as that observed *in vitro* in the absence of ATP (in rigor; Rayment *et al.* 1993*b*), and the light-chain or lever arm domain is assumed to tilt during the force generating working stroke (Rayment *et al.* 1993*b*; Dominguez *et al.* 1998; Irving *et al.* 2000; Geeves & Holmes, 2005). The orientation of the light chain domain is described by the angle θ between its long axis and the filament axis; θ increases during the working stroke (light grey to dark grey conformation in Fig. 5*A*). The shortening-step experiments showed that there are at least two populations of myosin heads during active isometric contraction at sarcomere length 2.1 μm: an actin-attached population with a relatively narrow axial mass distribution, and a detached population with a broader axial mass distribution and centre of mass displaced by about 2 nm towards the midpoint of the thick filament (Piazzesi *et al.* 2002, 2007; Reconditi *et al.* 2004; Huxley *et al.* 2006).

The fraction of myosin heads in these two populations has been estimated from the stiffness of the sarcomere in comparison to rigor conditions, in which all the heads are attached to actin (Cooke & Franks, 1980). In the present experiments, which used muscle fibres from *R. esculenta*, this fraction is 23% (Park-Holohan *et al.* 2012, and see Methods), slightly lower than in the *R. temporaria* fibres used in the previous experiments. The interference fine structure of the M3 reflection is also slightly different in the two species; in the present experiments R_{M3} during isometric contraction at sarcomere length 2.1 μm was 0.94 $\pm$ 0.02 (mean $\pm$ SEM, $n = 25$), compared with about 0.8 in *R. temporaria* (Piazzesi *et al.* 2002, 2007). The parameters in the two-population model of Piazzesi *et al.* (2007) were adapted to fit the mechanical and structural data for active isometric contraction at full filament overlap in *R. esculenta* as described in Methods. In these conditions the light chain domains of the 23% of myosin heads attached to actin have $\theta = 44°$, with a uniform angular dispersion of $\pm$ 17°, producing the axial mass distribution shown in Fig. 5*B* (black). The axial mass distribution of the 77% detached heads was represented as a Gaussian (Fig. 5*B*, grey) with centre 2.07 nm from the head–rod junction of the attached heads, and dispersion 3.6 nm, as in the previous model (Piazzesi *et al.* 2007).

The simplest interpretation of the sarcomere length-dependence of the M3 reflection during isometric contraction in terms of this two-population model of myosin head conformations would be that the attached fraction of myosin heads decreases with increasing sarcomere length in proportion to the available number of actin binding sites, i.e. to the overlap between thick and thin filaments. This interpretation assumes that detached myosin heads have the same conformation in the overlap and no-overlap regions of the thick filament. With this assumption, the two-population model clearly failed to fit the observed sarcomere length dependence of the intensity (I_{M3}; Fig. 5*D*) and interference fine structure (R_{M3}; Fig. 5*E*) of the M3 reflection during isometric contraction. The values of I_{M3} calculated from the two-population model (dashed line in Fig. 5*D*) are too high at the longer sarcomere lengths, and those of R_{M3} (dashed line in Fig. 5*E*) are much too low. We conclude that the detached myosin heads in the overlap and non-overlap regions of the thick filament must have different conformations.

The failure of the two-population model shows that there must be at least three populations of myosin heads during isometric contraction, with different conformations: actin-attached heads in the overlap zone (A heads), detached heads in the overlap zone and detached heads in the non-overlap zone. We previously proposed a three-population model to explain the changes in I_{M3} and R_{M3} following a step stretch of muscle fibres during active contraction at full filament overlap (Brunello *et al.* 2007). The model of Brunello *et al.* took into account the fact that each myosin molecule has two heads, and distinguished between partner or P heads (detached heads that are the partners of A heads) and D heads (detached heads in fully detached myosin molecules). The changes in the M3 reflection produced by a step stretch could be accurately reproduced by rapid attachment of the partner heads (Brunello *et al.* 2007). Since the concept of partner heads potentially provides a simple explanation for the presence of different head conformations in the overlap and non-overlap regions of the thick filament, we tested the ability of the three-population model of Brunello *et al.* (2007), with A, P and D heads, to fit the present data.

For *R. esculenta* muscle fibres during active isometric contraction at sarcomere length 2.1 μm, the appropriate parameters for the three-population model are: A heads (23%), $\theta = 55°$ with a uniform distribution of $\pm$ 17° (Fig. 5*C*, black); P heads (23%), $\theta = 72°$ with Gaussian

angular dispersion of 27° (Fig. 5*C*, thicker line, dark grey); D heads (54%), Gaussian mass distribution with the centre 2.0 nm from the head–rod junction of the attached heads and dispersion 5.46 nm (Fig. 5*C*, thinner line, light grey), as in Brunello *et al.* (2007; see Methods). The dispersion of the D heads is sufficiently large compared with their *ca* 14.5 nm axial repeat that they make almost no contribution to the M3 reflection; the D heads are highly disordered. This model was then applied to the sarcomere-length dependence of the M3 reflection during active isometric contraction under the assumption that the fractions of both the A and the P heads are directly proportional to the degree of overlap between thick and thin filaments, with all other heads including all those in the non-overlap region taking up the D conformation. With these assumptions, the three-population model of Brunello *et al.* accurately reproduced the observed sarcomere-length dependence of both I_{M3} and R_{M3} (Fig. 5*D* and *E*, continuous lines), supporting the conclusion that the head domains of myosin molecules that cannot bind to thin filaments during isometric contraction are highly disordered, in contrast to their ordered conformations in resting muscle.

Quasi-helical organisation of myosin heads and structure of the thick filament backbone

The first myosin layer line (ML1, Fig. 2*A* and *B*) is associated with the ordered quasi-helical tracks of the myosin heads on the surface of the thick filaments in resting muscle, and its intensity (I_{ML1}) has a characteristic dependence on sarcomere length (Fig. 6*A*). I_{ML1} is roughly constant in the sarcomere length range 2.1 to *ca* 2.6 μm,

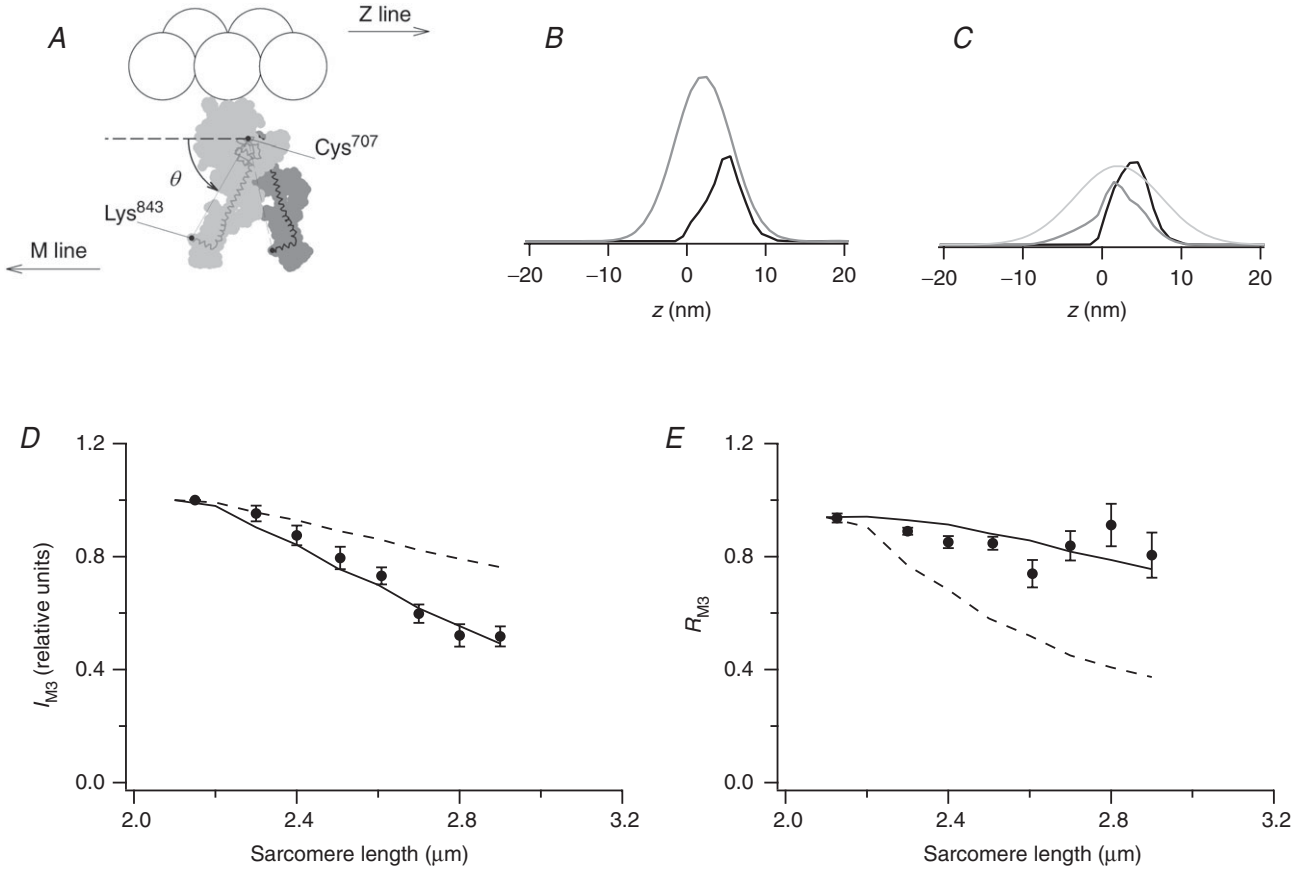

Figure 5. Model prediction of sarcomere length dependence of I_{M3} and R_{M3}
A, schematic of myosin head (grey) bound to actin (white circles) in two conformations, differing in the angle θ between the long axis of the light chain domain (Cys^{707}–Lys^{843}) and the actin filament axis (adapted from Reconditi *et al*. 2003). *B* and *C*, axial mass distributions at sarcomere length 2.1 μm of actin-attached (black) and detached (grey) myosin heads in the models with two (*B*) and three (*C*) head populations. Thick grey line in *C* denotes detached partners of actin-attached heads, and thin grey line detached myosin molecules. Zero on the abscissa corresponds to the position of Lys^{843}. *D* and *E*, comparison of experimental values of I_{M3} (*D*) and R_{M3} (*E*) (circles) in the sarcomere length range 2.1–2.9 μm with values calculated from the models with two and three populations of myosin heads (dashed and continuous lines, respectively). See text for details.

decreases between 2.6 and 3.0 μm, then is roughly constant again above 3.0 μm. The intensity of the M1 reflection (I_{M1}) associated with MyBP-C has a similar dependence on sarcomere length in resting fibres (Fig. 6*B*, open circles), as does that of the M5 reflection (I_{M5}, Fig. 6*C*), associated with the systematic axial perturbation of the three axial layers of myosin heads within each 43 nm repeat (Huxley & Brown, 1967; Squire, 1981) and the dominant peak of the M2 cluster (I_{M2}, not shown). The intensity decrease between 2.6 and 3.0 μm was most marked for the M1 and M5 reflections, which become weak at sarcomere lengths above 3.0 μm, whereas the intensities of the first myosin layer line and M2 reflection are reduced by about half at sarcomere lengths greater than 3.0 μm. In contrast, the intensity of the M6 reflection, I_{M6}, which is dominated by the periodic mass distribution of the filament backbone (Huxley *et al.* 2003, 2006), does not show the characteristic pattern of sarcomere length described above for the ML1, M1, M2 and M5 reflections in resting muscle, but increases slightly but continuously with increasing sarcomere length (Fig. 6*D*, open circles).

During isometric contraction, the M1 reflection (Fig. 6*B*, filled circles) is weaker than at rest (open circles) in the sarcomere length range 2.1–2.7 μm, but its intensity at longer lengths is independent of activation. The intensity of the M6 reflection, I_{M6}, is almost independent of sarcomere length during isometric contraction over the whole range studied (Fig. 6*D*, filled circles).

Thick filament periodicities

The spacings of the myosin-based meridional X-ray reflections give very precise measurements of the axial periodicities of the thick filaments and myosin heads. The sarcomere-length dependences of the spacings of the M2, M5 and M6 reflections in resting muscle (S_{M2}, S_{M5} and S_{M6}; Fig. 7*A*, *B* and *C*, respectively, open circles) were broadly similar to those of I_{ML1}, I_{M1}, I_{M2} and I_{M5} described above, i.e. they were roughly independent of sarcomere length in the range 2.1–2.6 μm, but become sarcomere length-dependent in the range 2.6–3.0 μm, in this case increasing at longer length. S_{M3} shows the same pattern (Fig. 4*D*, open circles), with little further change at lengths above 3.0 μm. S_{M2} and S_{M5} became difficult to measure precisely above sarcomere length 3.0 μm, but S_{M6} could be

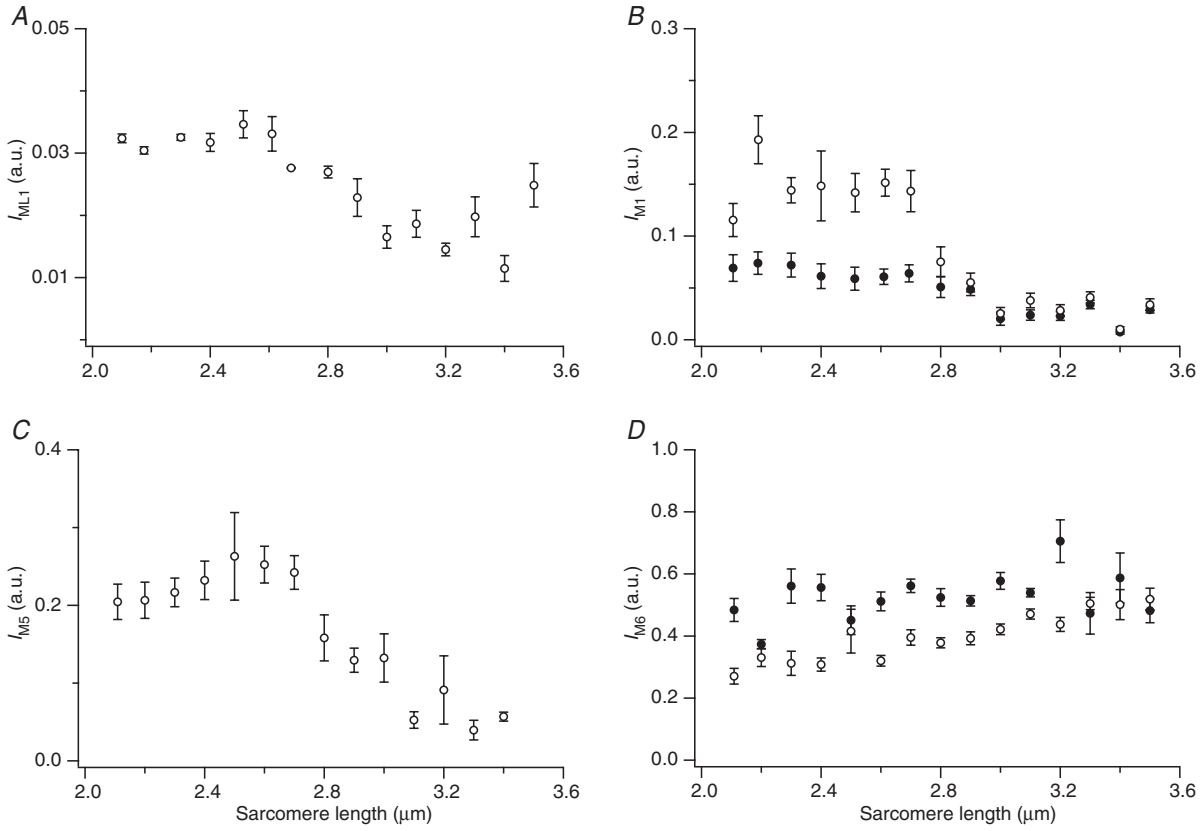

Figure 6. Sarcomere-length dependence of reflection intensities
Sarcomere-length dependence of the intensities of the ML1 (*A*), M1 (*B*), M5 (*C*) and M6 (*D*) reflections. Open symbols, at rest; filled symbols, isometric contraction.

measured reproducibly over the whole length range and seemed to increase further from 3.0 to 3.5 μm (Fig. 7*C*, open circles).

The values of S_{M2}, S_{M3}, S_{M5} and S_{M6} measured at short sarcomere lengths in resting muscle index quite well on the 43.02 nm myosin-based M1 periodicity characteristic of resting muscle (dashed lines in Figs 2*C* and *D*, 4*D* and 7). Thus, S_{M2} was close to 21.51 (43.02/2) nm (Fig. 7*A*), S_{M3} close to 14.34 (43.02/3) nm (Fig. 4*D*), S_{M5} close to 8.60 (43.02/5) nm (Fig. 7*B*) and S_{M6} close to 7.17 (43.02/6) nm (Fig. 7*C*). However, the fractional increase in spacing with increasing sarcomere length was different for the different reflections. S_{M6}, which is dominated by the contribution of the filament backbone, was 0.7% larger at sarcomere length 3.0 μm than at 2.5 μm, and the increases in S_{M2} and S_{M5}, although noisier, are consistent with this, indicating that all these reflections follow an underlying 0.7% increase in the periodicity of the thick filament backbone. In contrast, S_{M3}, which is dominated by the contribution of the myosin heads, was only about 0.3% larger at sarcomere length 3.0 μm than at 2.5 μm.

The sarcomere length dependence of S_{M3} during isometric contraction was described in an earlier section (Fig. 4*D*, filled circles). That of S_{M6} is similar (Fig. 7*C*, filled circles), i.e. almost independent of sarcomere length in the range 2.1 to *ca* 2.9 μm, then decreasing progressively with further increase in sarcomere length.

Discussion

Thick filament structure in resting muscle at short sarcomere length

In the sarcomere length range 2.1–2.6 μm, the thick filament-based meridional X-ray reflections in resting

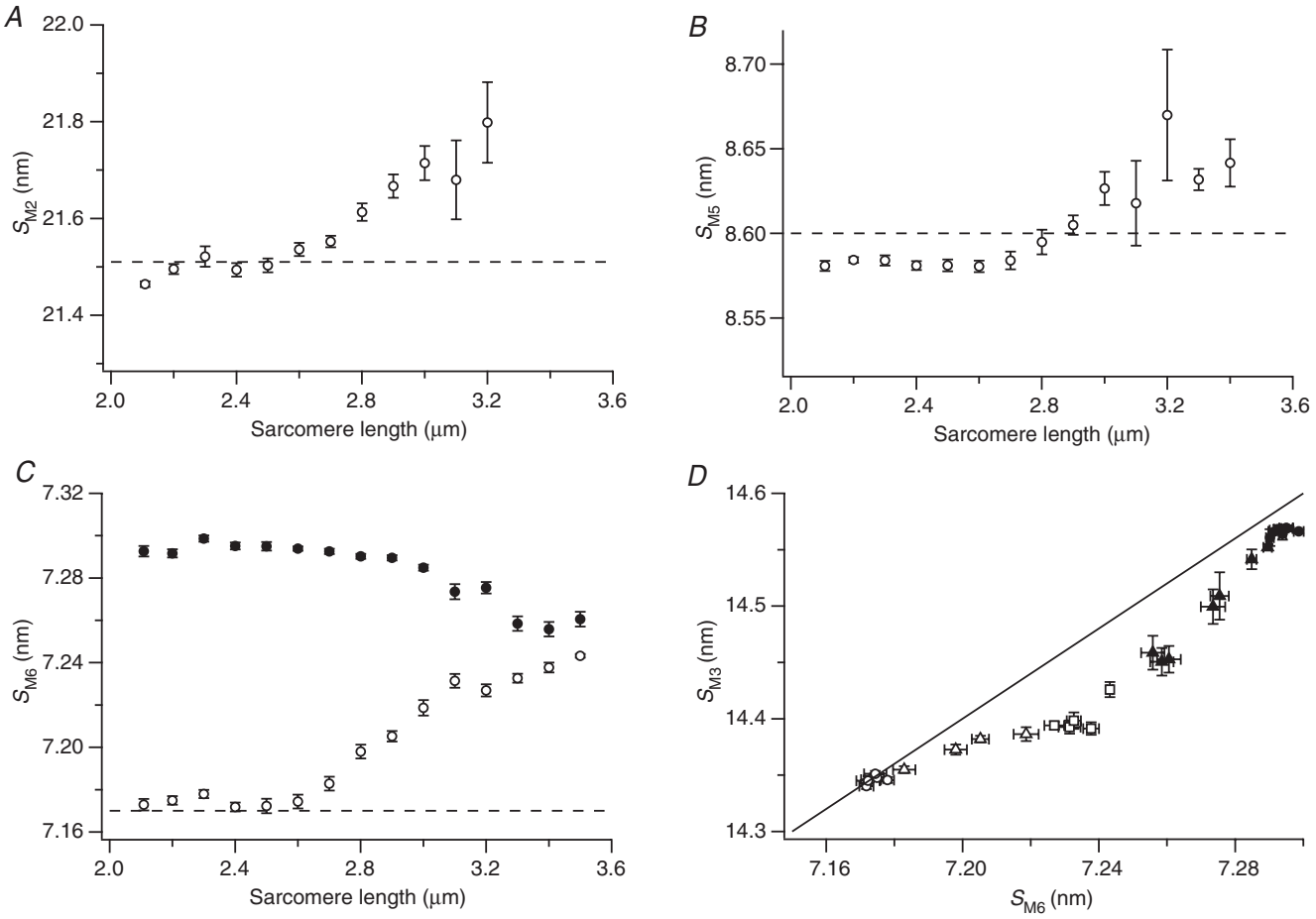

Figure 7. Sarcomere-length dependence of reflection spacings
Sarcomere-length dependence of the spacings of the M2 (*A*), M5 (*B*) and M6 (*C*) reflections and relationship between the spacings of the M3 and M6 reflections (*D*). In *A*–*C* horizontal dashed lines indicate the expected spacing of the reflections as orders of a 43.02 nm periodicity; open symbols, at rest; filled symbols, isometric contraction. In *D* for filled symbols, circles denote sarcomere length 2.1–2.9 μm and triangles 3.0–3.5 μm; for open symbols, circles denote sarcomere length 2.1–2.6 μm, triangles 2.7–3.0 μm and squares 3.1–3.5 μm.

muscle index quite accurately on a fundamental repeat of 43.02 nm. The myosin heads follow a set of three helical tracks on the surface of the filaments (Squire, 1981; Kensler & Stewart, 1983; Luther *et al.* 2011) with an overall 43 nm helical repeat, and this helical periodicity is responsible for the strong ML1 layer line reflection (Fig. 2*A* and *B*). However, a perfect three-start helix would not generate the meridional M1, M2, M4 or M5 X-ray reflections, which are therefore referred to as 'forbidden' reflections (Huxley & Brown, 1967). In general, the presence of relatively strong M1, M2, M4 and M5 reflections in resting muscle indicates that the mass distribution of the myosin heads or other filament components in each 43 nm axial period is not composed of three identical repeats of 14.34 nm (Squire, 1981; Malinchik & Lednev, 1992; Oshima *et al.* 2007, 2012; Luther *et al.* 2011). There are probably two effects: a contribution from proteins other than myosin with *ca* 43 nm axial periodicities, and systematic axial perturbations of the three layers of myosin heads within each 43 nm repeat. Both MyBP-C and titin have axial mass distributions with periodicities close to 43 nm in the C zone and the region between the C zone and the M line (Fig. 1; Bennett *et al.* 1986; Luther *et al.* 2008). MyBP-C in particular has a strong 43 nm periodicity in the C zone (Rome *et al.* 1973), and is therefore likely to make a large contribution to the M1 reflection and a smaller contribution to its second order, the M2 (Luther *et al.* 2008, 2011). On the other hand, the systematic perturbation of the three layers of heads in each 43 nm repeat, presumably mediated by myosin–MyBP-C or myosin–titin interactions, would be primarily responsible for the higher-order forbidden reflections such as the M5, with some contribution to the M2 (Malinchik & Lednev, 1992; Oshima *et al.* 2007, 2012).

Within each layer of myosin heads in resting muscle, the two heads of each myosin molecule are likely to form the J motif first described for smooth muscle myosin (Wendt *et al.* 2001), and subsequently observed by electron microscopy of isolated thick filaments from invertebrate skeletal muscle (Woodhead *et al.* 2005), mammalian cardiac muscle (Zoghbi *et al.* 2008) and intact sarcomeres of vertebrate skeletal muscle (Luther *et al.* 2011). The time course of the change in the interference fine structure of the M3 X-ray reflection during isometric force development at the start of tetanic stimulation is also consistent with the existence of the J motif in resting skeletal muscle (Reconditi *et al.* 2011).

The structure of the thick filaments of skeletal muscle is not yet known at high resolution, so the interpretations of the sarcomere length- and activation-related changes in the thick filament-based X-ray reflections presented below focus on correlations with muscle function, and in particular with muscle regulation, rather than on the details of thick filament structure.

Sarcomere-length dependence of thick filament structure in resting muscle and the role of MyBP-C

The intensities and spacings of the thick filament-based X-ray reflections are largely independent of sarcomere length in the range 2.1–2.6 μm in resting muscle (Figs 4*A*, 6 and 7, open circles). When the sarcomere length is increased from around 2.6–2.7 to 3.0 μm, corresponding approximately to the range in which the overlap between the thick filament C zone and the thin filaments is lost (Fig. 1), the intensities of the first myosin layer line (ML1) and the M1, M2 and M5 meridional reflections decrease (Fig. 6*A*–*C*), and the spacings of the meridional reflections increase (Figs 4*D* and 7, open circles). In contrast, the intensity and interference fine structure of the M3 reflection does not change (Fig. 4*A*), and the intensity of the M6 reflection increases slightly (Fig. 6*D*).

The large decrease in the intensity of the M1 reflection observed when the sarcomere length is increased from 2.6 to 3.0 μm (Fig. 6*B*) indicates that the periodic mass distribution of MyBP-C associated with this reflection is much less marked when the C zone does not overlap the thin filaments. This suggests that the strongly periodic mass distribution of MyBP-C in the C zone in resting muscle requires binding of MyBP-C to nearby actin filaments, and that such binding is associated with an MyBP-C orientation that is roughly perpendicular to the filament axis, so that a significant fraction of its mass becomes aligned with the 43 nm axial repeat of its binding site on the thick filaments.

The idea that MyBP-C, although constitutively a thick filament component, can also bind to actin was suggested soon after its initial characterization (Moos, 1981; Yamamoto, 1986), but the nature and physiological significance of such binding remain controversial (Pfuhl & Gautel 2012). Several *in vitro* studies have provided evidence that the N-terminal region of the cardiac isoform of MyBP-C can bind to actin filaments (Kulikovskaya *et al.* 2003; Shaffer *et al.* 2009; Kensler *et al.* 2011; Mun *et al.* 2011; Previs *et al.* 2012). However, the existence of extra domains and phosphorylation sites in the N-terminal region of the cardiac isoform means that these results cannot be reliably extrapolated to skeletal muscle. Moreover, whilst the C-terminal region of MyBP-C binds tightly to the thick filament backbone in both muscle types, the putative interaction of its N-terminal region with the thin filaments is relatively weak, and this region can also bind to myosin subfragment-2 (Ababou *et al.* 2008) and, at least in the cardiac system, to the myosin regulatory light chain (Ratti *et al.* 2011). In general, the idea that the N terminus of MyBP-C might bind either to the thin filament or to myosin is consistent with MyBP-C acting as a regulatory switch with the potential to signal between thin and thick filaments (Pfuhl & Gautel, 2012). The present results are consistent with the idea that MyBP-C binds

to thin filaments in resting skeletal muscle, as suggested by electron tomography of skeletal muscle rapidly frozen in the resting state (Luther *et al.* 2011).

The loss of the M1 X-ray reflection when resting sarcomeres are extended from 2.6 to 3.0 μm is accompanied by a large decrease in the intensity of the 'forbidden' M5 reflection and a smaller decrease in that of the M2 reflection associated with the systematic triplet perturbation of the three *ca* 14.34 nm layers of myosin heads within each 43 nm repeat. The increase in the intensity of the M6 reflection with increasing sarcomere length in this range may also be associated at least in part with the loss of the triplet perturbation. These results suggest that the triplet perturbation of the myosin head layers may be controlled by MyBP-C. When MyBP-C is in its actin-bound, perpendicular conformation, the triplet perturbation is maximised; when MyBP-C cannot bind actin, the triplet perturbation is lost. This coupling between MyBP-C and the triplet perturbations of the heads suggests a possible mechanism by which the three MyBP-C molecules could control the 18 myosin heads in each 43 nm layer of the C zone.

The intensity of the first myosin layer line (I_{ML1}; Fig. 6*A*) also decreased, by about 50%, as the sarcomere length was increased from 2.6 to 3.0 μm in resting muscle, indicating a correlated change in the helical arrangement of the heads on the surface of the filament, which might be associated with azimuthal motions of the heads in addition to the axial perturbations discussed above. The relatively small effect of stretching resting muscles to sarcomere lengths greater than 3.0 μm on the myosin-based layer lines including ML1 was first reported by Huxley (1972) and Haselgrove (1975), although those authors did not quantify the sarcomere-length dependence of the layer line intensities.

In contrast to the behaviour of the M1, ML1 and M5 reflections described above, the intensity and interference fine structure of the M3 reflection associated with the 14.34 nm axial periodicity of the heads (Fig. 4*A*) did not change with sarcomere length in the range 2.6–3.0 μm in resting muscle. Thus, the fundamental 14.34 nm periodic axial mass distribution of the heads, which we have argued is associated with the folded J-motif organization of pairs of myosin heads on the filament backbone, is precisely preserved in the presence of large changes in MyBP-C conformation and in the helical organisation of the myosin heads and their triplet perturbations.

In the sarcomere length range 3.0–3.5 μm, the intensities and spacings of the myosin-based meridional reflections and the first myosin layer line (ML1) were generally independent of sarcomere length in resting muscle, the only exceptions being I_{M6} and S_{M6} (Figs 6*D* and 7*C*, open circles), which seemed to increase slightly with increasing sarcomere length in this range. Thus, the structural changes in the thick filament described above are mainly confined to the range 2.6–3.0 μm, corresponding approximately to that in which the overlap between the thick filament C zone and thin filaments is removed.

Conformation of detached myosin heads during isometric contraction

The conformation of the detached myosin heads during isometric contraction was deduced from the sarcomere-length dependence of the M3 reflection, which allows the conformation of the heads in the region of the thick filament that overlaps with thin filaments to be distinguished from that of the heads in the non-overlap region which must be detached from actin. In the sarcomere length range 2.1–2.9 μm, the intensity of the M3 reflection (I_{M3}) is directly proportional to the degree of overlap between thick and thin filaments, as is active isometric force (Fig. 4*B*). Several effects preclude the accurate measurement of I_{M3} during active contraction at sarcomere lengths above about 2.9 μm. The intensity of the reflection becomes sensitive to the loss of lateral alignment between thick filaments (Fig. S1). Sarcomere homogeneity is lost (Fig. S5), due to dynamic instability between sarcomeres that can affect both I_{M3} and the interference fine structure of the M3 reflection (R_{M3}; Brunello *et al.* 2009). Finally, changes in the thick filament periodicity in this sarcomere length range indicated by S_{M3} (Fig. 4*D*) and S_{M6} (Fig. 7*C*) might affect I_{M3} and R_{M3}, as discussed below.

We therefore limited quantitative analysis and interpretation of the sarcomere length dependence of I_{M3} and R_{M3} during isometric contraction to the range 2.1–2.9 μm. In this range I_{M3} is proportional to the degree of overlap between thick and thin filaments, immediately suggesting that the myosin heads in the non-overlap region of the thick filament are axially disordered and make little or no contribution to the M3 reflection. Quantitative analysis of these results (Fig. 5) used models of myosin head conformations adapted from previous analyses of the changes in I_{M3} and R_{M3} produced by imposing rapid length changes during isometric contraction at sarcomere length 2.1 μm (Lombardi *et al.* 1995; Dobbie *et al.* 1998; Irving *et al.* 2000; Piazzesi *et al.* 2002; Reconditi *et al.* 2004; Huxley *et al.* 2006). The simplest model of this type, with a single conformation of detached myosin heads (Piazzesi *et al.* 2007), was unable to reproduce the sarcomere length-dependence of I_{M3} and R_{M3} (Fig. 5*D* and *E*, dashed lines). In contrast, a model with two types of detached head, developed originally to explain the changes in I_{M3} and R_{M3} in response to a rapid stretch (Brunello *et al.* 2007), gave a good fit to the sarcomere length-dependence of I_{M3} and R_{M3} (Fig. 5*D* and *E*, continuous lines). Thus, the present results provide further support for the proposal

(Brunello *et al.* 2007) that the detached partners of actin-attached heads have a conformation that is distinct from that of the heads of myosin molecules that are entirely detached from actin. Actin-attached heads constrain the relative conformation of their molecular partners, making their enzymatic and mechanical function as well as their conformation potentially different from that of the heads of detached myosin molecules (Brunello *et al.* 2007; Fusi *et al.* 2010). The latter are highly disordered, as indicated by their low contribution to I_{M3}, corresponding to a broad axial mass distribution, and may have distinct biochemical properties and be less available for rapid actin binding.

Implications of the changes in axial periodicities of the thick filament

The spacings of the M2, M5 and M6 reflections in resting muscle increase by *ca* 0.7% in the sarcomere length range 2.6–3.0 μm (Fig. 7*A*–*C*, open circles), suggesting that the backbone of the thick filament is elongated by 0.7%. An elongation of about the same size is observed when muscle fibres are put into rigor (Reconditi *et al.* 2003), and an elongation roughly twice as large (*ca* 1.5%) is observed on muscle activation at short sarcomere length (Fig. 7*C*; Haselgrove, 1975; Linari *et al.* 2000). The molecular structural basis of these periodicity changes is unknown, but they are not due to the elasticity of the thick filament (Huxley *et al.* 1994; Wakabayashi *et al.* 1994; Reconditi *et al.* 2004), and are probably associated with a change in the packing of the myosin tails in the filament backbone. The M3 reflection, which is dominated by the arrangement of the myosin heads on the surface of the filaments, exhibits a smaller spacing increase of *ca* 0.3% on stretch of resting muscle (Fig. 4*D*, open circles). Thus, the change in the axial periodicity of the heads does not completely follow that of the filament backbone. Such axial periodicity changes, at the level of either the heads or the backbone, could provide a co-operative mechanism for propagating structural changes along the thick filament, so that, for example, changes mediated by MyBP-C in the C zone might be spread to the whole 800 nm length of each half thick filament (Oshima *et al.* 2012).

During isometric contraction, the spacing of the M6 reflection (S_{M6}) *decreases* with increasing sarcomere length in the range 2.9–3.5 μm (Fig. 7*C*), opposite to the increase observed in resting muscle. The net result is that only a very small fraction of the *ca* 1.6% increase in backbone periodicity associated with activation at full filament overlap (sarcomere length 2.1 μm) remains at sarcomere length 3.5 μm. If the 7.17 nm value of S_{M6} in resting muscle at full filament overlap is considered to be a signature of the fully OFF state of the thick filament, and the 7.29 nm periodicity during steady isometric contraction at full overlap a signature of the ON state, the smaller values of S_{M6} observed during steady isometric contraction at sarcomere lengths greater than 2.9 μm suggest that the thick filaments are not fully ON in these conditions.

The behaviour of the M3 reflection during isometric contraction gives further support for this conclusion. The aberrant values of I_{M3} and R_{M3} at sarcomere lengths greater than 2.9 μm (Fig. 4*B* and *C*) could be explained by the presence of some resting-like myosin heads in the non-overlap region of the thick filament during activation. The axial periodicity of the myosin heads during isometric contraction, reported by the spacing of the M3 reflection, S_{M3} (Fig. 4*D*, filled circles), shows the same characteristic sarcomere-length dependence as that of the filament backbone reported by S_{M6} (Fig. 7*C*, filled circles), again in the opposite direction to the sarcomere-length dependence of S_{M3} in resting muscle. However, the ratio of the two periodicities is not constant, as shown more clearly by plotting S_{M3} against S_{M6} (Fig. 7*D*). Here, the spacing data from isometric contraction (filled symbols) and resting fibres (open symbols) at different sarcomere lengths define a clearly non-linear relationship between S_{M3} and S_{M6}.

In the sarcomere length range 2.1–2.6 μm, the S_{M3}/S_{M6} ratio in resting muscle is 2.0 (Fig. 7*D*, open circles). When the sarcomere length is increased from 2.6 to 3.0 μm (open triangles), MyBP-C links between the thick and thin filaments are lost and S_{M6} increases to 7.22 nm, but S_{M3} only increases to 14.38 nm, much less than expected from the expected 2:1 relationship between the two parameters. Thus, the myosin heads do not follow the increase in axial periodicity of the thick filament backbone in this range, probably because, as indicated by the constancy of both the intensity and the interference fine structure of the M3 reflection, the J-motif interactions between the two heads in each myosin molecule are retained up to the largest sarcomere length studied in resting muscle (3.5 μm), and these favour the lower value of S_{M3}. Further stretch of resting fibres from 3.0 to 3.5 μm (open squares) produced little further increase in S_{M3} apart from the single, possibly anomalous, point at 3.5 μm.

During steady isometric contraction in the sarcomere length range 2.1–2.9 μm (filled circles) S_{M3} is close to 14.56 nm, S_{M6} to 7.29 nm and the S_{M3}/S_{M6} ratio is again close to 2.0. At longer sarcomere lengths (filled triangles) S_{M6} and S_{M3} are smaller and S_{M3}/S_{M6} ratio is less than 2.0. Thus, as in resting muscle at sarcomere lengths greater than 2.6 μm, myosin heads do not follow the backbone periodicity during isometric contraction at sarcomere lengths greater than 2.9 μm. In these conditions, in which filament overlap is less than one-third of its maximum value, myosin heads in the non-overlap region of the thick filaments seem to revert partially to their ordered resting conformation, as already suggested above on the basis of the aberrant values of I_{M3} and R_{M3} (Fig. 4*B* and *C*). These resting-like heads are expected to have an axial periodicity

closer to 14.34 nm, explaining why the S_{M3}/S_{M6} ratio is less than 2.0.

It has been implicit in the above discussion that, up to 2.9 μm sarcomere length, S_{M3} and S_{M6} have the same value in the overlap and non-overlap regions of the filament. The alternative possibility, that during isometric contraction at reduced filament overlap the non-overlap region of the filament retains the 14.34/7.17 nm periodicities characteristic of resting muscle, is excluded by the constancy of S_{M3} and S_{M6} in the sarcomere length range 2.1–2.6 μm. The sarcomere length-independence of R_{M3} during isometric contraction in the range 2.1–2.9 μm (Fig. 4*C*) provides strong independent support for this conclusion, because even small changes in filament periodicity in the non-overlap region would change the phase of the interference splitting of the M3 reflection (Linari *et al.* 2000). It follows that both the conformation of the myosin heads in the non-overlap region, inferred in the previous section from the sarcomere length-dependence of I_{M3} and R_{M3}, and the periodicity of the filament backbone in the non-overlap region, inferred from that of S_{M6}, change on activation despite the absence of a local interaction with the thin filament.

Thick filament-based regulation in striated muscle

The results and interpretation presented above provide strong support for Haselgrove's (1975) hypothesis of a regulatory structural change in the thick filaments of vertebrate skeletal muscle, and reveal some of the molecular mechanisms involved. In the OFF state of the thick filament, myosin heads occupy J motifs packed against the filament backbone in quasi-helical tracks; the whole structure has a fundamental axial periodicity close to 43 nm, but the three layers of myosin heads in each 43 nm repeat are axially perturbed into non-equivalent triplets. This OFF structure of the thick filament is stabilised by interactions between MyBP-C and the thin filaments, and communicated along the filament by co-operative interactions between adjacent myosin heads, and/or between myosin tails in the filament backbone.

When muscle is activated by electrical stimulation, the structural changes in the thin filament following calcium binding are sensed by the MyBP-C links and communicated to the thick filaments, triggering a loss of the triplet perturbations of the myosin heads, a decrease in the helical order of the heads and an increase in thick filament periodicity. This combination of structural changes represents a 'partially ON' state of the thick filament that still has ordered myosin heads characterised by J motifs, and can be reproduced by stretching resting muscle fibres to sarcomere length 3.0 μm. Thus, an additional activation step or parallel signalling pathway that is coupled to the increase in cytoplasmic $[Ca^{2+}]$ through an unidentified mechanism is required to complete the ON state of the thick filament by disrupting the J motifs of resting myosin heads, allowing them to bind to actin and generate force.

This hypothetical sequence of events is supported by time-resolved X-ray studies of the structural changes accompanying muscle activation. The earliest structural changes are in the troponin reflections (Yagi, 2003; Matsuo & Yagi, 2008; Sugimoto *et al.* 2008; Matsuo *et al.* 2010), followed by almost synchronous changes in the second actin layer line associated with the azimuthal movement of tropomyosin (Kress *et al.* 1986; Matsuo & Yagi, 2008), the M1 reflection associated with the loss of the perpendicular conformation of MyBP-C and the axial periodicity of the thick filament measured by S_{M6} (Brunello *et al.* 2006; Reconditi *et al.* 2011). All these changes precede the changes in the interference fine structure of the M3 reflection that signals loss of the J motif, which are roughly synchronous with binding of myosin heads to actin and active force generation (Reconditi *et al.* 2011).

Such a thick filament-based regulatory mechanism is analogous to the primary control mechanism in smooth muscle, suggesting that a different signalling pathway may have evolved in vertebrate skeletal and cardiac muscles to control a similar conformational change in the myosin heads in the thick filaments. In striated muscles, such a thick filament-mediated pathway could modulate the fraction of myosin heads available to interact effectively with actin, reduce ATP hydrolysis by resting muscle (Stewart *et al.* 2010) and control the dynamics of muscle relaxation (Brunello *et al.* 2009). Further work will be required to test the hypothesis of thick filament regulation outlined above, and to better understand both its structural basis and its functional consequences.

References

Ababou A, Rostkova E, Mistry S, Le Masurier C, Gautel M & Pfuhl M (2008). Myosin binding protein C positioned to play a key role in regulation of muscle contraction: structure and interactions of domain C1. *J Mol Biol* **384**, 615–630.

Bennett P, Craig R, Starr R & Offer G (1986). The ultrastructural location of C-protein, X-protein and H-protein in rabbit muscle. *J Muscle Res Cell Motil* **7**, 550–567.

Bordas J, Mant GR, Diakun GP & Nave C (1987). X-ray diffraction evidence for the existence of 102.0- and 230.0-nm transverse periodicities in striated muscle. *J Cell Biol* **105**, 1311–1318.

Brunello E, Bianco P, Piazzesi G, Linari M, Reconditi M, Panine P, Narayanan T, Helsby WI, Irving M & Lombardi V (2006). Structural changes in the myosin filament and cross-bridge formation during the development of the isometric force in single fibres from frog muscle. *J Physiol* **577**, 971–984.

Brunello E, Reconditi M, Elangovan R, Linari M, Sun Y-B, Narayanan T, Panine P, Piazzesi G, Irving M & Lombardi V (2007). Skeletal muscle resists stretch by rapid binding of the second motor domain of myosin to actin. *Proc Natl Acad Sci U S A* **104**, 20114–20119.

Brunello E, Fusi L, Reconditi M, Linari M, Bianco P, Panine P, Narayanan T, Piazzesi G, Lombardi V & Irving M (2009). Structural changes in myosin motors and filaments during relaxation of skeletal muscle. *J Physiol* **587**, 4509–4521.

Cooke R & Franks K (1980). All myosin heads form bonds with actin in rigor rabbit skeletal muscle. *Biochemistry* **19**, 2265–2269.

Dobbie I, Linari M, Piazzesi G, Reconditi M, Koubassova N, Ferenczi MA, Lombardi V & Irving M (1998). Elastic bending and active tilting of myosin heads during muscle contraction. *Nature* **396**, 383–387.

Dominguez R, Freyzon Y, Trybus KM & Cohen C (1998). Crystal structure of a vertebrate smooth muscle myosin motor domain and its complex with the essential light chain: visualization of the pre-power stroke state. *Cell* **94**, 559–571.

Ebashi S, Endo M & Otsuki I (1969). Control of muscle contraction. *Q Rev Biophys* **4**, 351–384.

Elliott GF, Lowy J & Worthington CR (1963). An X-ray and light diffraction study of the filament lattice of striated muscle in the living state and in rigor. *J Mol Biol* **6**, 295–305.

Fusi L, Reconditi M, Linari M, Brunello E, Elangovan R, Lombardi V & Piazzesi G (2010). The mechanism of the resistance to stretch of isometrically contracting single muscle fibres. *J Physiol* **588**, 495–510.

Geeves MA & Holmes KC (2005). The molecular mechanism of muscle contraction. *Adv Protein Chem* **71**, 161–193.

Gordon AM, Homsher E & Regnier M (2000). Regulation of contraction in striated muscle. *Physiol Rev* **80**, 853–924.

Gordon AM, Huxley AF & Julian FJ (1966). The variation in isometric tension with sarcomere length in vertebrate muscle fibres. *J Physiol* **184**, 170–192.

Haselgrove JC (1975). X-ray evidence for conformational changes in the myosin filaments of vertebrate striated muscle. *J Mol Biol* **92**, 113–143.

Haselgrove J & Huxley HE (1973). X-ray evidence for radial cross-bridge movement and for the sliding filament model in actively contracting skeletal muscle. *J Mol Biol* **77**, 549–568.

Huxley AF & Lombardi V (1980). A sensitive force transducer with resonant frequency 50 kHz. *J Physiol* **305**, 15–16.

Huxley HE (1972). Structural changes in the actin- and myosin-containing filaments during contraction. *Cold Spring Harbor Symp Quant Biol* **37**, 361–376.

Huxley HE & Brown W (1967). The low angle x-ray diffraction diagram of vertebrate striated muscle and its behaviour during contraction and rigor. *J Mol Biol* **30**, 383–434.

Huxley HE, Faruqi AR, Kress M, Bordas J & Koch MHJ (1982). Time resolved x-ray diffraction studies of the myosin layer line reflections during muscle contraction. *J Mol Biol* **158**, 673–684.

Huxley HE, Stewart A, Sosa H & Irving T (1994). X-ray diffraction measurements of the extensibility of actin and myosin filaments in contracting muscle. *Biophys J* **67**, 2411–2421.

Huxley HE, Reconditi M, Stewart A & Irving T (2003). What the higher order meridional reflections tell us. *Biophys J* **84**, 139a.

Huxley HE, Reconditi M, Stewart A & Irving TC (2006). X-ray interference studies of crossbridge action in muscle contraction: evidence from quick releases. *J Mol Biol* **363**, 743–761.

Huxley HE, Reconditi M & Irving TC (2009). New X-ray data about myosin-binding protein C in frog muscle. *Biophys J* **96**, 616a.

Irving M, Piazzesi G, Lucii L, Sun Y-B, Harford JJ, Dobbie IM, Ferenczi MA, Reconditi M & Lombardi V (2000). Conformation of the myosin motor during force generation in skeletal muscle. *Nat Struct Biol* **7**, 482–485.

Kensler RW & Stewart M (1983). Frog skeletal muscle thick filaments are three-stranded. *J Cell Biol* **96**, 1797–1802.

Kensler RW, Shaffer JF& Harris SP (2011). Binding of the N-terminal fragment C0–C2 of cardiac MyBP-C to cardiac F-actin. *J Struct Biol* **174**, 45–51.

Kress M, Huxley HE, Faruqi AR & Hendrix J (1986). Structural changes during the activation of frog muscle studied by time-resolved x-ray diffraction. *J Mol Biol* **188**, 325–342.

Kulikovskaya I, McClellan G, Flavigny J, Carrier L & Winegrad S (2003). Effect of MyBP-C binding to actin on contractility in heart muscle. *J Gen Physiol* **122**, 761–774.

Linari M, Piazzesi G, Dobbie I, Koubassova N, Reconditi M, Narayanan T, Diat O, Irving M & Lombardi V (2000). Interference fine structure and sarcomere length dependence of the axial X-ray pattern from active single muscle fibres. *Proc Natl Acad Sci U S A* **97**, 7226–7231.

Lombardi V, Piazzesi G, Ferenczi MA, Thirlwell H, Dobbie I & Irving M (1995). Elastic distortion of myosin heads and repriming of the working stroke in muscle. *Nature* **374**, 553–555

Lowy J, Poulsen F (1990). Studies of the diffuse x-ray scattering from contracting frog skeletal muscles. *Biophys J* **57**, 977–985.

Luther PK, Bennett PM, Knupp C, Craig R, Padron R, Harris SP, Patel J & Moss RL (2008). Understanding the organization and role of myosin binding protein C in normal striated muscle by comparison with MyBP-C knockout cardiac muscle. *J Mol Biol* **384**, 60–72.

Luther PK, Winkler H, Taylor K, Zoghbi ME, Craig R, Padron R, Squire JM & Liu J (2011). Direct visualization of myosin-binding protein C bridging myosin and actin filaments in intact muscle. *Proc Natl Acad Sci U S A* **108**, 11423–11428.

Malinchik SB & Lednev VV (1992). Interpretation of the X-ray diffraction pattern from relaxed skeletal muscle and modelling of the thick filament structure. *J Muscle Res Cell Motil* **13**, 406–419.

Matsubara I & Elliott GE (1972). X-ray diffraction studies on skinned single fibres of frog skeletal muscle. *J Mol Biol* **72**, 657–669.

Matsuo T & Yagi N (2008). Structural changes in the muscle thin filament during contractions caused by single and double electrical pulses. *J Mol Biol* **383**, 1019–1036.

Matsuo T, Iwamoto H & Yagi N (2010). Monitoring the structural behavior of troponin and myoplasmic free Ca^{2+} concentration during twitch of frog skeletal muscle. *Biophys J* **99**, 193–200.

Moos C (1981). Fluorescence microscope study of the binding of added C protein to skeletal muscle myofibrils. *J Cell Biol* **90**, 25–31.

Mun JY, Gulick J, Robbins J, Woodhead J, Lehman W & Craig R (2011). Electron microscopy and 3D reconstruction of F-actin decorated with cardiac myosin-binding protein C (cMyBP-C). *J Mol Biol* **410**, 214–225.

Oshima K, Takezawa Y, Sugimoto Y, Kobayashi T, Irving TC & Wakabayashi K (2007). Axial dispositions and conformations of myosin crossbridges along thick filaments in relaxed and contracting states of vertebrate striated muscles by X-ray fiber diffraction. *J Mol Biol* **367**, 275–301.

Oshima K, Sugimoto Y, Irving TC & Wakabayashi K (2012). Head–head interactions of resting myosin crossbridges in intact frog skeletal muscles, revealed by synchrotron X-ray fiber diffraction. *PLoS One* **7**, e52421.

Park-Holohan S, Linari M, Reconditi M, Fusi L, Brunello E, Irving M, Dolfi M, Lombardi V, West TG, Curtin NA, Woledge RC & Piazzesi G (2012). Mechanics of myosin function in white muscle fibres of the dogfish, *Scyliorhinus canicula*. *J Physiol* **590**, 1973–1988.

Pfuhl M & Gautel M (2012). Structure, interactions and function of the N-terminus of cardiac myosin binding protein C (MyBP-C): who does what, with what, and to whom? *J Muscle Res Cell Motil* **33**, 83–94.

Piazzesi G, Reconditi M, Dobbie I, Linari M, Boesecke P, Diat O, Irving M & Lombardi V (1999). Changes in conformation of myosin heads during the development of isometric contraction and rapid shortening in single frog muscle fibres. *J Physiol* **514**, 305–312.

Piazzesi G, Reconditi M, Linari M, Lucii L, Sun Y-B, Narayanan T, Boesecke P, Lombardi V & Irving M (2002). Mechanism of force generation by myosin heads in skeletal muscle. *Nature* **415**, 659–662.

Piazzesi G, Reconditi M, Linari M, Lucii L, Bianco P, Brunello E, Decostre V, Stewart A, Gore DB, Irving TC, Irving M & Lombardi V (2007). Skeletal muscle performance determined by modulation of number of myosin motors rather than motor force or stroke size. *Cell* **131**, 784–795.

Previs MJ, Beck Previs S, Gulick J, Robbins J & Warshaw DM (2012). Molecular mechanics of cardiac myosin-binding protein C in native thick filaments. *Science* **337**, 1215–1218.

Ratti J, Rostkova E, Gautel M & Pfuhl M (2011). Structure and interactions of myosin-binding protein C domain C0: cardiac-specific regulation of myosin at its neck? *J Biol Chem* **286**, 12650–12658.

Rayment I, Rypniewski W, Schmidt-Base K, Smith R, Tomchick DR, Benning MM, Winkelmann DA, Wesenberg G, Holden HM (1993*a*). Three dimensional structure of myosin subfragment-1: a molecular motor. *Science* **261**, 50–58.

Rayment I, Holden HM, Whittaker M, Yohn CB, Lorenz M, Holmes KC, Milligan RA (1993*b*). Structure of the actin–myosin complex and its implications for muscle contraction. *Science* **261**, 58–65.

Reconditi M, Koubassova N, Linari M, Dobbie I, Narayanan T, Diat O, Piazzesi G, Lombardi V & Irving M (2003). The conformation of myosin head domains in rigor muscle determined by X-ray interference. *Biophys J* **85**, 1098–1110.

Reconditi M, Linari M, Lucii L, Stewart A, Sun Y-B, Boesecke P, Narayanan T, Fischetti RF, Irving T, Piazzesi G, Irving M & Lombardi V (2004). The myosin motor in muscle generates a smaller and slower working stroke at higher load. *Nature* **428**, 578–581.

Reconditi M, Brunello E, Linari M, Bianco P, Narayanan T, Panine P, Piazzesi G, Lombardi V & Irving M (2011). Motion of myosin head domains during activation and force development in skeletal muscle. *Proc Natl Acad Sci U S A* **108**, 7236–7240.

Rome E, Offer G & Pepe FA (1973). X-ray diffraction of muscle labelled with antibody to C-protein. *Nat New Biol* **244**, 152–154.

Shaffer JF, Kensler RW & Harris SP (2009). The myosin binding protein C motif binds to F-actin in a phosphorylation-sensitive manner. *J Biol Chem* **284**, 12318–27.

Squire, JM (1981). *The Structural Basis of Muscle Contraction*. Plenum Press, New York.

Stewart MA, Franks-Skiba K, Chen S, Cooke, R (2010). Myosin ATP turnover is a mechanism involved in thermogenesis in skeletal muscle fibers. *Proc Natl Acad Sci U S A* **107**, 430–435.

Sugimoto Y, Takezawa Y, Matsuo T, Ueno Y, Minakata S, Tanaka H & Wakabayashi K (2008). Structural changes of the regulatory proteins bound to the thin filaments in skeletal muscle contraction by X-ray fiber diffraction. *Biochem Biophys Res Commun* **369**, 100–108.

Sztucki M, Dicola E & Narayanan T (2010). Instrumental developments for anomalous small-angle X-ray scattering from soft matter systems. *J Appl Cryst* **3**, 1479–1487

Wakabayashi K, Sugimoto Y, Tanaka H, Ueno Y, Takezawa Y & Amemiya Y (1994). X-ray diffraction evidence for the extensibility of actin and myosin filaments during muscle contraction. *Biophys J* **67**, 2422–2435.

Wendt T, Taylor D, Trybus KM & Taylor K (2001). Three dimensional image reconstruction of dephosphorylated smooth muscle heavy meromyosin reveals asymmetry in the interaction between myosin heads and placement of subfragment 2. *Proc Natl Acad Sci U S A* **98**, 4361–4366.

Woodhead JL, Zhao F-Q, Craig R, Egelman EH, Alamo L & Padron R (2005). Atomic model of a myosin filament in the relaxed state. *Nature* **436**, 1195–1199.

Yagi N (2003). An X-ray diffraction study on early structural changes in skeletal muscle contraction. *Biophys J* **84**, 1093–1102.

Yamamoto K (1986.) The binding of skeletal muscle C-protein to regulated actin. *FEBS Lett* **208**, 123–127.

Zoghbi ME, Woodhead JL, Moss RL & Craig R (2008). Three-dimensional structure of vertebrate cardiac muscle filaments. *Proc Natl Acad Sci U S A* **105**, 2386–2390.

Additional information

Competing interests

None declared.

Author contributions

The experiments were performed at the ESRF. M.R., E.B., L.F., M.L., V.L., M.I. and G.P. contributed to the conception and design of the experiments, the collection, analysis and interpretation of data, and drafting the article or revising it critically for important intellectual content. M.F.M. contributed to data collection. All authors approved the final version of the manuscript, all persons designated as authors qualify for authorship and all those who qualify for authorship are listed.

Funding

Financial support was provided by Ente Cassa di Risparmio di Firenze, FIRB-Futuro in Ricerca project RBFR08JAMZ and MIUR-PRIN project 2010R8JK2X (Italy), MRC (UK), Royal Society (UK), Wellcome Trust (UK) and ESRF.

Acknowledgements

We thank M. Dolfi and J. Gorini for electronic and mechanical engineering support, and T. Narayanan for optimising performance of the X-ray beamline and help with data collection.